Applied Mathematical Modelling 36 (2012) 1431–1443

Contents lists available at SciVerse ScienceDirect

Applied Mathematical Modelling

journal homepage: www.elsevier.com/locate/apm

Exact solution of transient thermal stress problem of a multilayered magneto-electro-thermoelastic hollow sphere

Yoshihiro Ootao *, Masayuki Ishihara

Department of Mechanical Engineering, Graduate School of Engineering, Osaka Prefecture University, 1-1 Gakuen-cho, Nakaku, Sakai 599-8531, Japan

ARTICLE INFO

Article history:
Received 23 December 2010
Accepted 31 August 2011
Available online 7 September 2011

Keywords:
Thermal stress problem
Magneto-electro-thermoelastic
Hollow sphere
Spherically symmetric problem
Transient state

ABSTRACT

This paper presents the theoretical analysis of a multilayered magneto-electro-thermoelastic hollow sphere under unsteady and uniform surface heating. We obtain the exact solution of the transient thermal stress problem of the multilayered magneto-electro-thermoelastic hollow sphere in the spherically symmetric state. As an illustration, we perform numerical calculations of a two-layered composite hollow sphere made of piezoelectric and magnetostrictive materials and investigate the numerical results for temperature change, displacement, stress, and electric and magnetic potential distributions in the transient state are shown in figures.

1. Introduction

It has recently been found that composites made of piezoelectric and magnetostrictive materials exhibit the magnetoelectric effect, which is not seen in piezoelectric or magnetostrictive materials [1–3]. These materials are known as multiferroic composites [4]. These composites exhibit a coupling among magnetic, electric, and elastic fields. It is possible to develop a new system of smart composite materials by combining these piezoelectric and magnetostrictive materials with other structural materials.

In the past, various problems in magneto-electro-elastic media that exhibit anisotropic and linear coupling among the magnetic, electric, and elastic fields were analyzed. Examples of static problems are as follows. Pan [5] derived the exact solution of simply supported and multilayered magneto-electro-elastic plates, and Pan and Heyliger [6] derived the exact solution of magneto-electro-elastic laminates in cylindrical bending. Babaei and Chen [7] derived the exact solution of radially polarized and magnetized rotating magneto-electro-elastic hollow and solid cylinders. Ying and Wang [8] derived the exact solution of rotating magneto-electro-elastic composite hollow cylinders. Wang et al. [9] derived an analytical solution of a multilayered magneto-electro-elastic circular plate under simply supported boundary conditions. Examples of dynamic problems are as follows. Wang and Ding [10] analyzed the transient responses of a magneto-electro-elastic hollow sphere and a magneto-electro-elastic composite hollow sphere [11] subjected to spherically symmetric dynamic loads. Anandkumar et al. [12] analyzed the free vibration behavior of multiphase and layered magneto-electro-elastic beams.

Examples of thermal stress problems are as follows. Sunar et al. [13] analyzed thermopiezomagnetic smart structures and Kumaravel et al. [14] analyzed a three-layered electro-magneto-elastic strip under steady state conditions using the finite element method. Hou et al. [15] obtained 2D fundamental solutions of a steady point heat source in infinite and semi-infinite orthotropic electro-magneto-thermo-elastic planes and obtained Green's function for a steady point heat source on the

* Corresponding author. Tel.: +81 72 254 9208; fax: +81 72 254 9904.
E-mail address: ootao@me.osakafu-u.ac.jp (Y. Ootao).

0307-904X/$ - see front matter © 2011 Elsevier Inc. All rights reserved.
doi:10.1016/j.apm.2011.08.043

surface of a semi-infinite transversely isotropic electro-magneto-thermo-elastic material [16]. Xiong and Ni [17] obtained 2D Green's functions for semi-infinite transversely isotropic electro-magneto-thermo-elastic composites. Gao et al. [18] analyzed the problem of collinear cracks in an electro-magneto-thermo-elastic solid subjected to uniform heat flow at infinity. These studies, however, treated thermal stress problems only under steady temperature distribution. It is well known that thermal stress distributions in a transient state show significant and large response values as compared to those in a steady state. Therefore, transient thermoelastic problems are important. With regard to transient thermal stress problems, Wang and Niraula [19] analyzed transient thermal fracture in transversely isotropic electro-magneto-elastic cylinders. The exact solution of a transient analysis of multilayered magneto-electro-thermoelastic strip subjected to nonuniform heat supply was also obtained [20]. However, to the best of the authors' knowledge, the exact analysis of a multilayered magneto-electro-thermoelastic hollow sphere under unsteady heat supply has not yet been reported. Here, we present the derivation of an exact solution of the transient thermal stress problem of a multilayered composite hollow sphere made of magneto-electro-thermoelastic materials under uniform surface heating in a spherically symmetric state. We assumed that the magneto-electro-thermoelastic materials are polarized and magnetized in the radial direction.

2. Analysis

We considered a multilayered composite hollow sphere made of spherical isotropic and linear magneto-electro-thermoelastic materials. The hollow sphere's inner and outer radii are denoted by a and b, respectively. r_i is the outer radius of the ith layer. Throughout this article, indices i (=1,2,...,N) are associated with the ith layer from the inner side of a composite hollow sphere.

2.1. Heat conduction problem

We assumed that the multilayered hollow sphere is initially at zero temperature and its the inner and outer surfaces are suddenly heated by surrounding media having constant temperatures T_a and T_b with relative heat transfer coefficients h_a and h_b, respectively. Then, the temperature distribution is one-dimensional and the transient heat conduction equation for the ith layer is written in the following form:

$$\frac{\partial \overline{T}_i}{\partial \tau} = \bar{\kappa}_{ri}\left(\frac{\partial^2 \overline{T}_i}{\partial \bar{r}^2} + \frac{2}{\bar{r}}\frac{\partial \overline{T}_i}{\partial \bar{r}}\right); \quad i = 1,\ldots,N. \tag{1}$$

The initial and thermal boundary conditions in dimensionless form are

$$\tau = 0; \quad \overline{T}_i = 0; \quad i = 1,2,\ldots,N, \tag{2}$$

$$\bar{r} = \bar{a}; \quad \frac{\partial \overline{T}_1}{\partial \bar{r}} - H_a\overline{T}_1 = -H_a\overline{T}_a, \tag{3}$$

$$\bar{r} = R_i; \quad \overline{T}_i = \overline{T}_{i+1}; \quad i = 1,2,\ldots,N-1, \tag{4}$$

$$\bar{r} = R_i; \quad \bar{\lambda}_{ri}\frac{\partial \overline{T}_i}{\partial \bar{r}} = \bar{\lambda}_{r,i+1}\frac{\partial \overline{T}_{i+1}}{\partial \bar{r}}; \quad i = 1,2,\ldots,N-1, \tag{5}$$

$$\bar{r} = 1; \quad \frac{\partial \overline{T}_N}{\partial \bar{r}} + H_b\overline{T}_N = H_b\overline{T}_b. \tag{6}$$

In Eqs. (1)–(6), we introduced the following dimensionless values:

$$\begin{aligned} &(\overline{T}_i, \overline{T}_a, \overline{T}_b) = (T_i, T_a, T_b)/T_0, \quad (\bar{r}, R_i, \bar{a}) = (r, r_i, a)/b, \quad \tau = \kappa_0 t/b^2, \\ &\bar{\kappa}_{ri} = \kappa_{ri}/\kappa_0, \quad \bar{\lambda}_{ri} = \lambda_{ri}/\lambda_0, \quad (H_a, H_b) = (h_a, h_b)b, \end{aligned} \tag{7}$$

where T_i is the temperature change; t is time; and T_0, λ_0 and κ_0 are typical values of temperature, thermal conductivity, and thermal diffusivity, respectively. Introducing the Laplace transform with respect to the variable τ, the solution of Eq. (1) can be obtained so as to satisfy the conditions (2)–(6). This solution is written as follows:

$$\overline{T}_i = \frac{1}{F}\left(\overline{A}_i' + \frac{\overline{B}_i'}{\bar{r}}\right) + \sum_{j=1}^{\infty}\frac{2\exp\left(-\mu_j^2\tau\right)}{\mu_j \Delta'(\mu_j)}\left[\overline{A}_i j_0(\beta_i\mu_j\bar{r}) + \bar{B}_i y_0(\beta_i\mu_j\bar{r})\right]; \quad i = 1,2,\ldots,N, \tag{8}$$

where $j_0()$ and $y_0()$ are zeroth-order Spherical Bessel functions of the first and second kind, respectively. Furthermore, Δ and F are the determinants of $2N \times 2N$ matrice $[a_{kl}]$ and $[e_{kl}]$, respectively; the coefficients $\overline{A}_i$ and $\overline{B}_i$ are defined as determinants of a matrix similar to the coefficient matrix $[a_{kl}]$, in which the $(2i-1)$th column or $2i$th column is replaced with the constant vector $\{c_k\}$, respectively. Similarly, the coefficients $\overline{A}_i'$ and $\overline{B}_i'$ are defined as determinants of a matrix similar to the coefficient matrix $[e_{kl}]$, in which the $(2i-1)$th column or $2i$th column is replaced with the constant vector $\{c_k\}$, respectively. The nonzero elements of the coefficient matrices $[a_{kl}]$ and $[e_{kl}]$ and the constant vector $\{c_k\}$ are given as

$$a_{1,1} = \beta_1\mu j_1(\beta_1\mu\bar{a}) + H_a j_0(\beta_1\mu\bar{a}), \quad a_{1,2} = \beta_1\mu y_1(\beta_1\mu\bar{a}) + H_a y_0(\beta_1\mu\bar{a}),$$

$$a_{2N,2N-1} = H_b j_0(\beta_N\mu) - \beta_N\mu j_1(\beta_N\mu), \quad a_{2N,2N-1} = H_b y_0(\beta_N\mu) - \beta_N\mu y_1(\beta_N\mu),$$

$$a_{2i,2i-1} = j_0(\beta_i\mu R_i), \quad a_{2i,2i} = y_0(\beta_i\mu R_i), \quad a_{2i,2i+1} = -j_0(\beta_{i+1}\mu R_i), \quad a_{2i,2i+2} = -y_0(\beta_{i+1}\mu R_i), \tag{9}$$

$$a_{2i+1,2i-1} = -\bar{\lambda}_{ri}\beta_i\mu j_1(\beta_i\mu R_i),$$

$$a_{2i+1,2i} = -\bar{\lambda}_{ri}\beta_i\mu y_1(\beta_i\mu R_i), \quad a_{2i+1,2i+1} = \bar{\lambda}_{r,i+1}\beta_{i+1}\mu j_1(\beta_{i+1}\mu R_i),$$

$$a_{2i+1,2i+2} = \bar{\lambda}_{r,i+1}\beta_{i+1}\mu y_1(\beta_{i+1}\mu R_i); \quad i = 1,2,\ldots,N-1 \tag{10}$$

$$e_{1,1} = H_a, \quad e_{1,2} = \frac{1}{\bar{a}^2}(1 + H_a\bar{a}), \quad e_{2N,2N-1} = H_b, \quad e_{2N,2N} = H_b - 1 \tag{11}$$

$$\begin{aligned} &e_{2i,2i-1} = 1, \quad e_{2i,2i} = \frac{1}{R_i}, \quad e_{2i,2i+1} = -1, \quad e_{2i,2i+2} = -\frac{1}{R_i}, \\ &e_{2i+1,2i} = \frac{\bar{\lambda}_{ri}}{R_i^2}, \quad e_{2i+1,2i+1} = -\frac{\bar{\lambda}_{r,i+1}}{R_i^2}; \quad i = 1,2,\ldots,N-1 \end{aligned} \tag{12}$$

$$c_1 = H_a\overline{T}_a, \quad c_{2N} = H_b\overline{T}_b, \tag{13}$$

In Eq. (8), $\Delta'(\mu_j)$ is

$$\Delta'(\mu_j) = \left.\frac{d\Delta}{d\mu}\right|_{\mu=\mu_j} \tag{14}$$

and μ_j is the jth positive root of the following transcendental equation:

$$\Delta(\mu) = 0. \tag{15}$$

2.2. Thermoelastic problem

We developed the analysis of a multilayered magneto-electro-thermoelastic hollow sphere as a spherically symmetric state. The displacement–strain relations are expressed in dimensionless form as follows:

$$\bar{\varepsilon}_{rri} = \bar{u}_{ri,\bar{r}}, \quad \bar{\varepsilon}_{\theta\theta i} = \bar{\varepsilon}_{\phi\phi i} = \bar{u}_{ri}/\bar{r}, \quad \bar{\gamma}_{r\theta i} = \bar{\gamma}_{r\phi i} = \bar{\gamma}_{\theta\phi i} = 0, \tag{16}$$

where the comma denotes partial differentiation with respect to the variable that follows. For the spherical isotropic and linear magneto-electro-thermoelastic materials, the constitutive relations are expressed in dimensionless form as follows:

$$\begin{aligned} &\bar{\sigma}_{rri} = \overline{C}_{11i}\bar{\varepsilon}_{rri} + 2\overline{C}_{12i}\bar{\varepsilon}_{\theta\theta i} - \bar{\beta}_{ri}\overline{T}_i - \bar{e}_{1i}\overline{E}_{ri} - \bar{q}_{1i}\overline{H}_{ri}, \\ &\bar{\sigma}_{\theta\theta i} = \bar{\sigma}_{\phi\phi i} = \overline{C}_{12i}\bar{\varepsilon}_{rri} + (\overline{C}_{22i} + \overline{C}_{23i})\bar{\varepsilon}_{\theta\theta i} - \bar{\beta}_{\theta i}\overline{T}_i - \bar{e}_{2i}\overline{E}_{ri} - \bar{q}_{2i}\overline{H}_{ri}, \end{aligned} \tag{17}$$

where

$$\begin{aligned} &\bar{\beta}_{ri} = \overline{C}_{11i}\bar{\alpha}_{ri} + 2\overline{C}_{12i}\bar{\alpha}_{\theta i}, \\ &\bar{\beta}_{\theta i} = \overline{C}_{12i}\bar{\alpha}_{ri} + (\overline{C}_{22i} + \overline{C}_{23i})\bar{\alpha}_{\theta i}. \end{aligned} \tag{18}$$

The constitutive equations for the electric and the magnetic fields in dimensionless form are given as

$$\overline{D}_{ri} = \bar{e}_{1i}\bar{\varepsilon}_{rri} + 2\bar{e}_{2i}\bar{\varepsilon}_{\theta\theta i} + \bar{\eta}_{1i}\overline{E}_{ri} + \bar{d}_{1i}\overline{H}_{ri} + \bar{p}_{1i}\overline{T}_i, \tag{19}$$

$$\overline{B}_{ri} = \bar{q}_{1i}\bar{\varepsilon}_{rri} + 2\bar{q}_{2i}\bar{\varepsilon}_{\theta\theta i} + \bar{d}_{1i}\overline{E}_{ri} + \bar{\mu}_{1i}\overline{H}_{ri} + \bar{m}_{1i}\overline{T}_i. \tag{20}$$

The relation between the electric field intensity and the electric potential ϕ_i in dimensionless form is defined as

$$\overline{E}_{ri} = -\bar{\phi}_{i,\bar{r}}. \tag{21}$$

The relation between the magnetic field intensity and the magnetic potential ψ_i in dimensionless form is defined as s

$$\overline{H}_{ri} = -\bar{\psi}_{i,\bar{r}}. \tag{22}$$

The equilibrium equation in the radial direction is expressed in dimensionless form as follows:

$$\bar{\sigma}_{rri,\bar{r}} + 2(\bar{\sigma}_{rri} - \bar{\sigma}_{\theta\theta i})/\bar{r} = 0. \tag{23}$$

If the electric charge density is zero, the equations of electrostatics and magnetostatics are expressed in dimensionless form as follows:

$$\overline{D}_{ri,\bar{r}} + 2\overline{D}_{ri}/\bar{r} = 0, \tag{24}$$

$$\overline{B}_{ri,\bar{r}} + 2\overline{B}_{ri}/\bar{r} = 0. \tag{25}$$

In Eqs. (16)–(25), the following dimensionless values are introduced:

$$\begin{aligned}
&\bar{\sigma}_{kli} = \frac{\sigma_{kli}}{\alpha_0 Y_0 T_0}, \quad (\bar{\varepsilon}_{kli}, \bar{\gamma}_{kli}) = \frac{(\varepsilon_{kli}, \gamma_{kli})}{\alpha_0 T_0}, \quad \bar{u}_{ri} = \frac{u_{ir}}{\alpha_0 T_0 b}, \quad \bar{\alpha}_{ki} = \frac{\alpha_{ki}}{\alpha_0}, \quad \overline{C}_{kli} = \frac{C_{kli}}{Y_0},\\
&\overline{D}_{ri} = \frac{D_{ri}}{\alpha_0 Y_0 T_0 |d_0|}, \quad \overline{B}_{ri} = \frac{B_{ri}|d_0|\kappa_0}{b\alpha_0 T_0}, \quad \bar{\phi}_i = \frac{\phi_i |d_0|}{\alpha_0 T_0 b}, \quad \bar{\psi}_i = \frac{\psi_i}{|d_0|\kappa_0\alpha_0 Y_0 T_0},\\
&\bar{e}_{ki} = \frac{e_{ki}}{Y_0|d_0|}, \quad \bar{\eta}_{1i} = \frac{\eta_{1i}}{Y_0|d_0|^2}, \quad \bar{q}_{ki} = \frac{q_{ki}\kappa_0|d_0|}{b}, \quad \bar{\mu}_{1i} = \frac{\mu_{1i}\kappa_0^2|d_0|^2 Y_0}{b^2},\\
&\bar{d}_{1i} = \frac{\kappa_0 d_{1i}}{b}, \quad \bar{p}_{1i} = \frac{p_{1i}}{\alpha_0 Y_0|d_0|}, \quad \bar{m}_{1i} = \frac{m_{1i}\kappa_0|d_0|}{b\alpha_0}, \quad \overline{E}_{ri} = \frac{E_{ri}|d_0|}{\alpha_0 T_0},\\
&\overline{H}_{ri} = \frac{H_{ri} b}{|d_0|\kappa_0\alpha_0 Y_0 T_0},
\end{aligned} \tag{26}$$

where σ_{kli} are the stress components; $(\varepsilon_{kli}, \gamma_{kli})$ are the strain components; u_{ri} is the displacement in the r direction; α_{ki} are the coefficients of linear thermal expansion; C_{kli} are the elastic stiffness constants; D_{ri} is the electric displacement in the r direction; B_{ri} is the magnetic flux density in the r direction; e_{ki} are the piezoelectric coefficients; η_{1i} is the dielectric constant; p_{1i} is the pyroelectric constant; q_{ki} are the piezomagnetic coefficients; μ_{1i} is the magnetic permeability coefficient; d_{1i} is the magnetoelectric coefficient; m_{1i} is the pyromagnetic constant; and α_0, Y_0, and d_0 are typical values of the coefficient of linear thermal expansion, Young's modulus and piezoelectric modulus, respectively.

Substituting Eqs. (16), (21) and (22) into Eqs. (17), (19) and (20), and later into Eqs. (23)–(25), the governing equations of the displacement u_{ri}, electric potential ϕ_i, and magnetic potential ψ_i in the dimensionless form are written as

$$\begin{aligned}
&\overline{C}_{11i}\bar{u}_{ri,\bar{r}\bar{r}} + 2\overline{C}_{11i}\bar{u}_{ri,\bar{r}}\bar{r}^{-1} + 2(\overline{C}_{12i} - \overline{C}_{22i} - \overline{C}_{23i})\bar{u}_{ri}\bar{r}^{-2} + \bar{e}_{1i}\bar{\phi}_{i,\bar{r}\bar{r}} + 2(\bar{e}_{1i} - \bar{e}_{2i})\bar{\phi}_{i,\bar{r}}\bar{r}^{-1} + \bar{q}_{1i}\bar{\psi}_{i,\bar{r}\bar{r}} + 2(\bar{q}_{1i} - \bar{q}_{2i})\bar{\psi}_{i,\bar{r}}\bar{r}^{-1}\\
&\quad = 2(\bar{\beta}_{ri} - \bar{\beta}_{0i})\overline{T}_i\bar{r}^{-1} + \bar{\beta}_{ri}\overline{T}_{i,\bar{r}},
\end{aligned} \tag{27}$$

$$\bar{e}_{1i}\bar{u}_{ri,\bar{r}\bar{r}} + 2(\bar{e}_{1i} + \bar{e}_{2i})\bar{u}_{ri,\bar{r}}\bar{r}^{-1} + 2\bar{e}_{2i}\bar{u}_{ri}\bar{r}^{-2} - \bar{\eta}_{1i}\bar{\phi}_{i,\bar{r}\bar{r}} - 2\bar{\eta}_{1i}\bar{\phi}_{i,\bar{r}}\bar{r}^{-1} - \bar{d}_{1i}\bar{\psi}_{i,\bar{r}\bar{r}} - 2\bar{d}_{1i}\bar{\psi}_{i,\bar{r}}\bar{r}^{-1} = -\bar{p}_{1i}(\overline{T}_{i,\bar{r}} + 2\overline{T}_i\bar{r}^{-1}), \tag{28}$$

$$\bar{q}_{1i}\bar{u}_{ri,\bar{r}\bar{r}} + 2(\bar{q}_{1i} + \bar{q}_{2i})\bar{u}_{ri,\bar{r}}\bar{r}^{-1} + 2\bar{q}_{2i}\bar{u}_{ri}\bar{r}^{-2} - \bar{d}_{1i}\bar{\phi}_{i,\bar{r}\bar{r}} - 2\bar{d}_{1i}\bar{\phi}_{i,\bar{r}}\bar{r}^{-1} - \bar{\mu}_{1i}\bar{\psi}_{i,\bar{r}\bar{r}} - 2\bar{\mu}_{1i}\bar{\psi}_{i,\bar{r}}\bar{r}^{-1} = -\bar{m}_{1i}(\overline{T}_{i,\bar{r}} + 2\overline{T}_i\bar{r}^{-1}). \tag{29}$$

If the inner and outer surfaces of the multilayered magneto-electro-thermoelastic hollow sphere are traction free, and the interfaces of each adjoining layer are perfectly bonded, then the boundary conditions of inner and outer surfaces and the conditions of continuity at the interfaces can be represented as follows:

$$\begin{aligned}
&\bar{r} = \bar{a}; \quad \bar{\sigma}_{rr1} = 0,\\
&\bar{r} = R_i; \quad \bar{\sigma}_{rri} = \bar{\sigma}_{rr,i+1}, \quad \bar{u}_{ri} = \bar{u}_{r,i+1}; \quad i = 1, \ldots, N-1,\\
&\bar{r} = 1; \quad \bar{\sigma}_{rrN} = 0.
\end{aligned} \tag{30}$$

The boundary conditions in the radial direction for the electric and magnetic fields are expressed as

$$\begin{aligned}
&\bar{r} = \bar{a}; \quad \overline{D}_{r1} = 0, \overline{B}_{r1} = 0 \quad \text{or} \quad \bar{\phi}_1 = 0, \bar{\psi}_1 = 0,\\
&\bar{r} = R_i; \quad \overline{D}_{ri} = \overline{D}_{r,i+1}, \quad \overline{B}_{ri} = \overline{B}_{r,i+1}, \quad \bar{\phi}_i = \bar{\phi}_{i+1}, \quad \bar{\psi}_i = \bar{\psi}_{i+1}; \quad i = 1, \ldots, N-1,\\
&\bar{r} = 1; \quad \overline{D}_{rN} = 0, \quad \overline{B}_{rN} = 0 \quad \text{or} \quad \bar{\phi}_N = 0, \quad \bar{\psi}_N = 0.
\end{aligned} \tag{31}$$

The solutions of Eqs. (27)–(29) are assumed in the following form:

$$\bar{u}_{ri} = \bar{u}_{rci} + \bar{u}_{rpi}, \quad \bar{\phi}_i = \bar{\phi}_{ci} + \bar{\phi}_{pi}, \quad \bar{\psi}_i = \bar{\psi}_{ci} + \bar{\psi}_{pi} \tag{32}$$

In Eq. (32), the first term on the right-hand side gives the homogeneous solution and the second term gives the particular solution. The homogeneous solutions of Eq. (32) can be expressed as follows:

$$\begin{aligned}
&\bar{u}_{rci} = C_{1i}\bar{r}^{-1} + C_{2i}\bar{r}^{\lambda_{i2}} + C_{3i}\bar{r}^{\lambda_{i3}},\\
&\bar{\phi}_{ci} = \frac{\overline{C}_{11i}}{\bar{e}_{1i}}(C_{6i} + C_{7i}\bar{r}^{-1} + g_{1i}C_{2i}\bar{r}^{\lambda_{i2}} + g_{2i}C_{3i}\bar{r}^{\lambda_{i3}}),\\
&\bar{\psi}_{ci} = \frac{\overline{C}_{11i}}{\bar{q}_{1i}}(C_{4i} + C_{5i}\bar{r}^{-1} + g_{3i}C_{2i}\bar{r}^{\lambda_{i2}} + g_{4i}C_{3i}\bar{r}^{\lambda_{i3}}),
\end{aligned} \tag{33}$$

where

$$
\begin{aligned}
&\lambda_{i2},\lambda_{i3}=\frac{-1\pm\sqrt{1-4b_{1i}/b_{3i}}}{2},\\
&b_{1i}=-\left[\alpha_i\gamma_i+\beta_{ei}^2-\beta_{ei}-\frac{\beta_{qi}\gamma_i-\beta_{ei}\beta_{di}}{\delta_i\gamma_i-\beta_{di}^2}(\gamma_i-\beta_{di}-\beta_{qi}\gamma_i+\beta_{ei}\beta_{di})\right],\\
&b_{3i}=1+\gamma_i+\frac{(\gamma_i-\beta_{di})^2}{\delta_i\gamma_i-\beta_{di}^2},\\
&\alpha_i=\frac{2(\overline{C}_{22i}+\overline{C}_{23i}-\overline{C}_{12i})}{\overline{C}_{11i}},\quad \beta_{ei}=\frac{2\bar{e}_{2i}}{\bar{e}_{1i}},\quad \beta_{qi}=\frac{2\bar{q}_{2i}}{\bar{q}_{1i}},\quad \beta_{di}=\frac{\overline{C}_{11i}\bar{d}_{1i}}{\bar{e}_{1i}\bar{q}_{1i}},\\
&\bar{\gamma}_i=\frac{\overline{C}_{11i}\bar{\eta}_{1i}}{\bar{e}_{1i}^2},\quad \delta_i=\frac{\overline{C}_{11i}\bar{\mu}_{1i}}{\bar{q}_{1i}^2},\\
&g_{1i}=\frac{1}{\gamma_i\lambda_{i2}(\lambda_{i2}+1)}\left[\lambda_{i2}^2+\lambda_{i2}+\beta_{ei}(\lambda_{i2}+1)-\beta_{di}\lambda_{i2}a_{3i}\right],\\
&g_{2i}=\frac{1}{\gamma_i\lambda_{i3}(\lambda_{i3}+1)}\left[\lambda_{i3}^2+\lambda_{i3}+\beta_{ei}(\lambda_{i3}+1)-\beta_{di}\lambda_{i3}a_{4i}\right],\\
&g_{3i}=a_{3i}/(\lambda_{i2}+1),\quad g_{4i}=a_{4i}/(\lambda_{i3}+1),\\
&a_{3i}=\frac{\lambda_{i2}+1}{\lambda_{i2}(\delta_i\gamma_i-\beta_{di}^2)}[(\gamma_i-\beta_{di})\lambda_{i2}+\beta_{qi}\gamma_i-\beta_{ei}\beta_{di}],\\
&a_{4i}=\frac{\lambda_{i3}+1}{\lambda_{i3}(\delta_i\gamma_i-\beta_{di}^2)}[(\gamma_i-\beta_{di})\lambda_{i3}+\beta_{qi}\gamma_i-\beta_{ei}\beta_{di}]
\end{aligned}
\tag{34}
$$

In Eq. (33), $C_{ki}(k=1,2,\ldots,7)$ are unknown constants. We have the following relation:

$$-\alpha_iC_{1i}+\beta_{ei}C_{7i}+\beta_{qi}C_{5i}=0. \tag{35}$$

In order to obtain the particular solutions, series expansions of Sphere Bessel functions given in Eq. (8) are used. Eq. (8) can be written in the following way:

$$\overline{T}_i(\bar{r}_i,\tau)=\sum_{n=0}^{\infty}\left[a_{in}(\tau)\bar{r}^{2n}+b_{in}(\tau)\bar{r}^{2n-1}\right], \tag{36}$$

where

$$
\begin{aligned}
a_{in}(\tau)&=\frac{\overline{A}_i'}{F}\delta_{0n}+\sum_{j=1}^{\infty}\overline{A}_i\frac{2\exp\left(-\mu_j^2\tau\right)}{\mu_j\Delta'(\mu_j)}\cdot\frac{(-1)^n\left(\beta_i\mu_j\right)^{2n}}{(2n+1)!},\\
b_{in}(\tau)&=\frac{\overline{B}_i'}{F}\delta_{0n}+\sum_{j=1}^{\infty}\overline{B}_i\frac{2\exp\left(-\mu_j^2\tau\right)}{\mu_j\Delta'(\mu_j)}\cdot\frac{(-1)^{n+1}(\beta_i\mu_j)^{2n-1}}{(2n)!}.
\end{aligned}
\tag{37}
$$

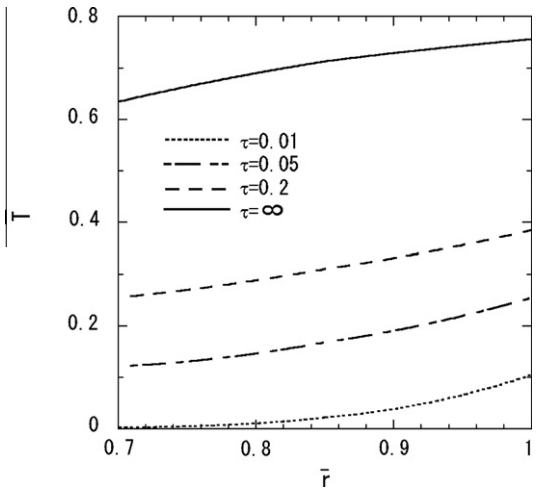

Fig. 1. Variation of temperature change in the radial direction (Case 1, $R_1 = 0.85$).

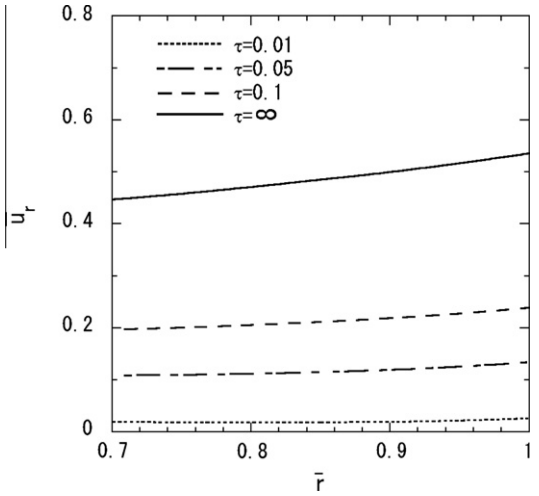

Fig. 2. Variation of displacement $\bar{u}_r$ in the radial direction (Case 1, $R_1 = 0.85$).

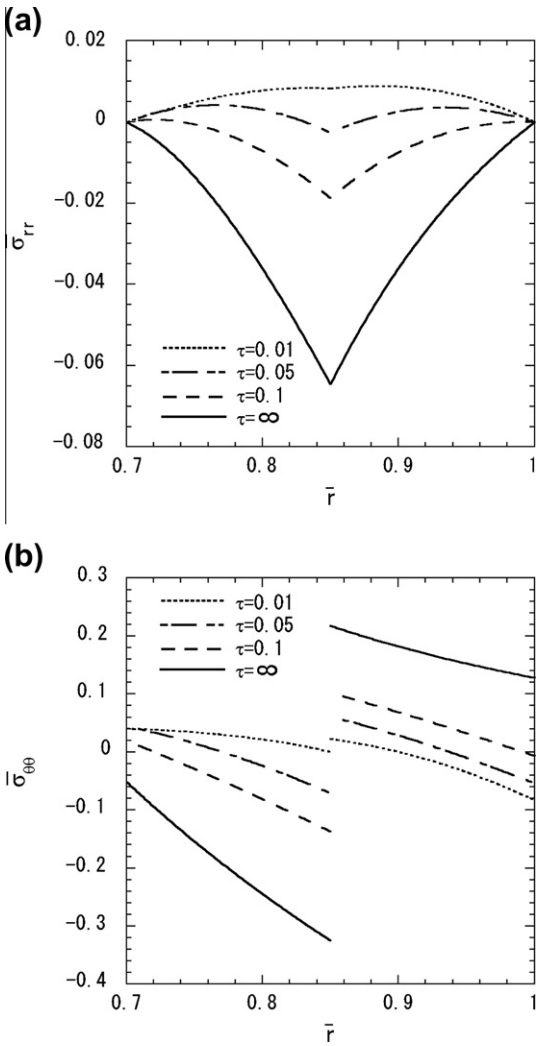

Fig. 3. Variation of thermal stresses in the radial direction (Case 1, $R_1 = 0.85$): (a) normal stress $\bar{\sigma}_{rr}$ and (b) normal stress $\bar{\sigma}_{\theta\theta}$.

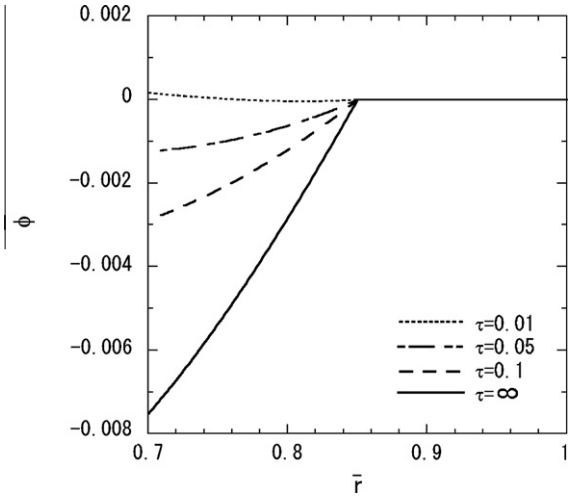

Fig. 4. Variation of electric potential in the radial direction (Case 1, $R_1 = 0.85$).

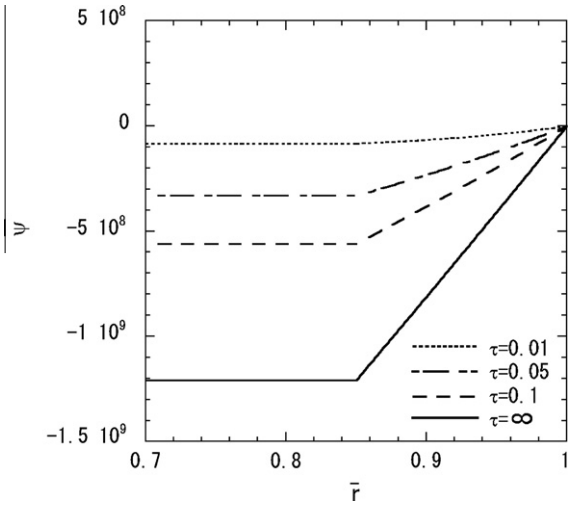

Fig. 5. Variation of magnetic potential in the radial direction (Case 1, $R_1 = 0.85$).

Here, δ_{0n} is the Kronecker delta. The particular solutions $\bar{u}_{rpi}$, $\bar{\phi}_{pi}$, and $\bar{\psi}_{pi}$ are obtained in the following forms:

$$\begin{aligned}
\bar{u}_{rip} &= \sum_{n=0}^{\infty} \left[f_{ani}(\tau)\bar{r}^{2n+1} + f_{bni}(\tau)\bar{r}^{2n} \right], \\
\bar{\phi}_{ip} &= \sum_{n=0}^{\infty} \left[h_{ani}(\tau)\bar{r}^{2n+1} + h_{bni}(\tau)\bar{r}^{2n} \right] + h_{c0i}(\tau)\ln\bar{r}, \\
\bar{\psi}_{ip} &= \sum_{n=0}^{\infty} \left[g_{ani}(\tau)\bar{r}^{2n+1} + g_{bni}(\tau)\bar{r}^{2n} \right] + g_{c0i}(\tau)\ln\bar{r}.
\end{aligned} \tag{38}$$

Expressions for $f_{ani}(\tau)$, $f_{bni}(\tau)$, $h_{ani}(\tau)$, $h_{bni}(\tau)$, $h_{c0i}(\tau)$, $g_{ani}(\tau)$, $g_{bni}(\tau)$, and $g_{c0i}(\tau)$ in Eq. (38) have been omitted here for brevity. Then, the stress components, electric displacement, and the magnetic flux density can be evaluated from Eq. (33). Details of the solutions are omitted from here for brevity. The unknown constants in the homogeneous solutions are determined so as to satisfy the boundary conditions in (30) and (31).

3. Numerical results

In order to illustrate the foregoing analysis, we consider a two-layered hollow sphere composed of piezoelectric and magnetostrictive layers. The piezoelectric layer is made up of $BaTiO_3$, and the magnetostrictive layer is made up of $CoFe_2O_4$. Two

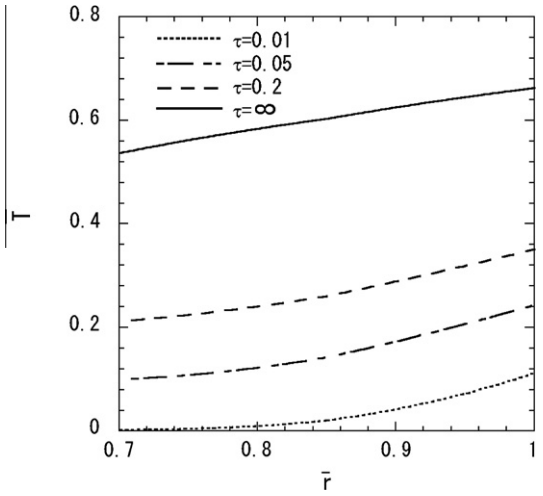

Fig. 6. Variation of temperature change in the radial direction (Case 2, $R_1 = 0.85$).

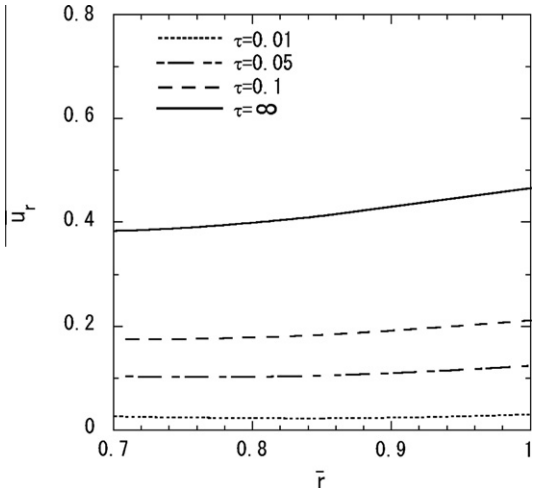

Fig. 7. Variation of displacement $\bar{u}_r$ in the radial direction (Case 2, $R_1 = 0.85$).

kinds of two-layered hollow sphere are investigated. Case 1 shows the stacking sequence $BaTiO_3/CoFe_2O_4$ and Case 2 shows the stacking sequence $CoFe_2O_4/BaTiO_3$. We assume that the outer surface of the two-layered hollow sphere is heated. Then, numerically calculable parameters of the heat condition and shape are presented as follows:

$$\begin{aligned} &H_a = H_b = 1.0, \quad \overline{T}_a = 0, \quad \overline{T}_b = 1, \quad N = 2, \\ &\bar{a} = 0.7, \quad R_1 = 0.75, 0.8, 0.85, 0.9, 0.95, \quad b = 0.01m \end{aligned} \tag{39}$$

The following are material constants considered for $BaTiO_3$ [20]:

$$\begin{aligned} &\alpha_\theta = \alpha_\phi = 15.7 \times 10^{-6} 1/\mathrm{K}, \quad \alpha_r = 6.4 \times 10^{-6} 1/\mathrm{K}, \\ &C_{22} = 166\ \mathrm{GPa}, \quad C_{23} = 77\ \mathrm{GPa}, \quad C_{12} = 78\ \mathrm{GPa}, \quad C_{11} = 162\ \mathrm{GPa} \\ &e_2 = -4.4\ \mathrm{C/m^2}, \quad e_1 = 18.6\ \mathrm{C/m^2}, \quad \eta_1 = 12.6 \times 10^{-9}\ \mathrm{C^2/Nm^2}, \\ &p_1 = 2 \times 10^{-4}\ \mathrm{C^2/m^2K}, \quad \mu_1 = 10 \times 10^{-6}\ \mathrm{Ns^2/C^2}, \quad \lambda_r = 2.5\ \mathrm{W/mK}, \\ &\kappa_r = 0.88 \times 10^{-6}\ \mathrm{m^2/s}. \end{aligned} \tag{40}$$

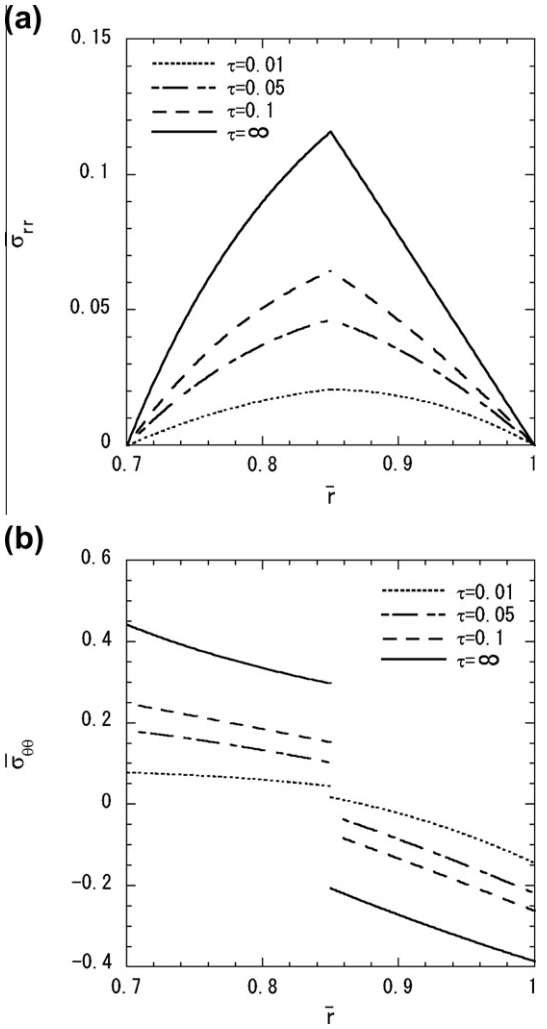

Fig. 8. Variation of thermal stresses in the radial direction (Case 2, $R_1 = 0.85$): (a) normal stress $\bar{\sigma}_{rr}$ and (b) normal stress $\bar{\sigma}_{\theta\theta}$.

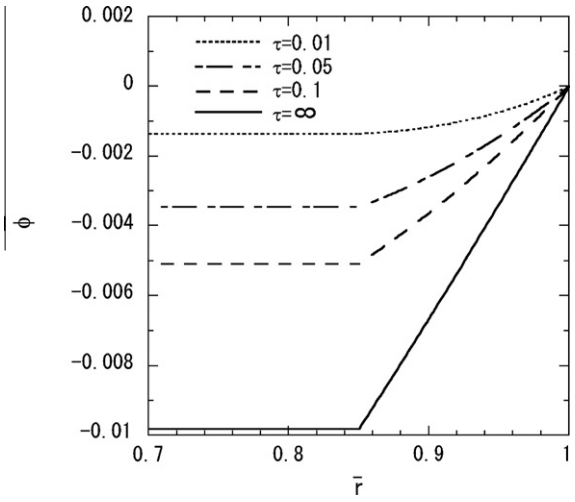

Fig. 9. Variation of electric potential in the radial direction (Case 2, $R_1 = 0.85$).

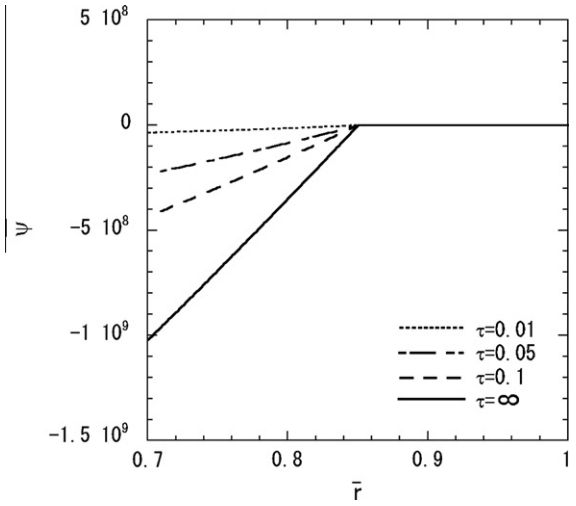

Fig. 10. Variation of magnetic potential in the radial direction (Case 2, $R_1 = 0.85$).

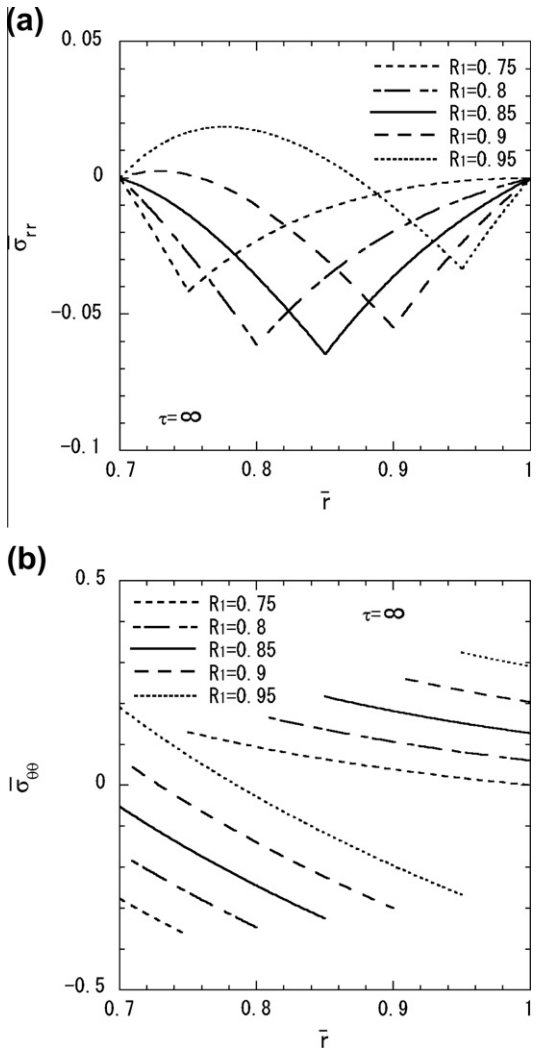

Fig. 11. Variation of thermal stresses in the radial direction (Case 1, $\tau = \infty$): (a) normal stress $\bar{\sigma}_{rr}$ and (b) normal stress $\bar{\sigma}_{\theta\theta}$.

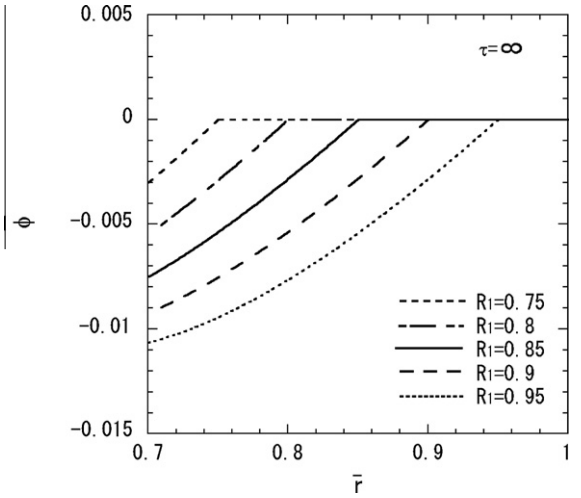

Fig. 12. Variation of electric potential in the radial direction (Case 1, $\tau = \infty$).

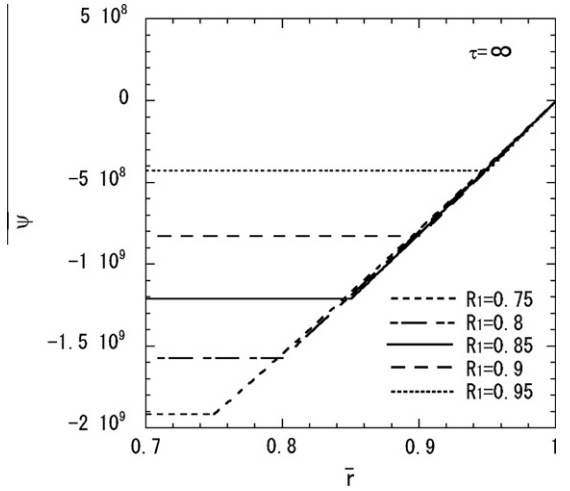

Fig. 13. Variation of magnetic potential in the radial direction (Case 1, $\tau = \infty$).

The corresponding constants for $CoFe_2O_4$ are

$$\begin{aligned}
&\alpha_r = \alpha_\theta = \alpha_\phi = 10 \times 10^{-6} 1/\mathrm{K}, \quad C_{22} = 286\ \mathrm{GPa},\\
&C_{23} = 173\ \mathrm{GPa}, \quad C_{12} = 170.5\ \mathrm{GPa}, \quad C_{11} = 269.5\ \mathrm{GPa},\\
&q_2 = 580.3\ \mathrm{N/Am}, \quad q_1 = 699.7\ \mathrm{N/Am}, \quad \eta_1 = 0.093 \times 10^{-9}\ \mathrm{C^2/Nm^2},\\
&p_1 = 2 \times 10^{-4}\ \mathrm{C^2/m^2K}, \quad \mu_1 = 157 \times 10^{-6}\ \mathrm{Ns^2/C^2}, \quad \lambda_r = 3.2\ \mathrm{W/mK},\\
&\kappa_r = 0.77 \times 10^{-6}\ \mathrm{m^2/s}.
\end{aligned} \tag{41}$$

The typical values of material parameters such as κ_0, λ_0, α_0, Y_0, and d_0, used to normalize the numerical data, based on those of $BaTiO_3$ are as follows:

$$\kappa_0 = \kappa_r, \quad \lambda_0 = \lambda_r, \quad \alpha_0 = \alpha_r, \quad Y_0 = 116\ \mathrm{GPa}, \quad d_0 = -78 \times 10^{-12}\ \mathrm{C/N}. \tag{42}$$

In the numerical calculations, the boundary conditions at the surfaces for the electric and magnetic fields are expressed as

$$\begin{aligned}
&\bar{r} = \bar{a}; \quad \overline{D}_{r1} = 0, \quad \overline{B}_{r1} = 0,\\
&\bar{r} = 1; \quad \bar{\phi}_N = 0, \quad \bar{\psi}_N = 0.
\end{aligned} \tag{43}$$

The numerical results for Case 1 and $R_1 = 0.85$ are shown in Figs. 1–5. Fig. 1 shows the variation of temperature change along the radial direction. Fig. 2 shows the variation of displacement $\bar{u}_r$ along the radial direction. From Figs. 1 and 2, it is clear that the temperature and displacement increase with time and have the largest values in steady state. Fig. 3(a) and (b) shows

variations of thermal stresses $\bar{\sigma}_{rr}$ and $\bar{\sigma}_{\theta\theta}$, respectively, along the radial direction. Fig. 3(a) reveals that the maximum tensile stress occurs in the transient state and the maximum compressive stress occurs in the steady state. From Fig. 3(b), it is clear that the compressive stress occurs in the first layer and tensile stress occurs in the second layer. Figs. 4 and 5 show variations of electric potential $\bar{\phi}$ and magnetic potential $\bar{\psi}$, respectively, along the radial direction. Fig. 4 reveals that the absolute value of the electric potential increases with time, except during the early stage of heating, and attains its maximum value in the steady state. The electric potential is almost zero in the second layer, i.e. the magnetostrictive layer. From Fig. 5, it is clear that the absolute value of the magnetic potential increases with time and attains its maximum value in the steady state. The magnetic potential is almost constant in the first layer, i.e. the piezoelectric layer.

The numerical results for Case 2 and $R_1 = 0.85$ are shown in Figs. 6–10. Fig. 6 shows the variation of temperature change along the radial direction. Fig. 7 shows the variation of displacement $\bar{u}_r$ along the radial direction. From Figs. 1, 2, 6 and 7, it is clear that the temperature increase and displacement $\bar{u}_r$ of Case 1 are larger than those of Case 2. Fig. 8(a) and (b) shows the variations of thermal stresses $\bar{\sigma}_{rr}$ and $\bar{\sigma}_{\theta\theta}$, respectively, along the radial direction. From Fig. 8(a), it is clear that the maximum tensile stress occurs in the steady state. Fig. 8(b) reveals that tensile stress occurs in the first layer and compressive stress occurs in the second layer. Figs. 9 and 10 show the variations of electric potential $\bar{\phi}$ and magnetic potential $\bar{\psi}$, respectively, along the radial direction. From these figures, it is clear that the absolute values of the electric and the magnetic potential increases with time and attain their maximum value in the steady state. The electric potential is almost constant in the first layer, i.e. the magnetostrictive layer. In contrast, the magnetic potential is almost zero in the second layer, i.e. the piezoelectric layer.

In order to assess the influence of the position of the interface between both layers, numerical results for Case 1 and $R_1 = 0.75, 0.8, 0.85, 0.9, 0.95$ were obtained; these results are shown in Figs. 11–13. Fig. 11(a) and (b) shows the variations of thermal stresses $\bar{\sigma}_{rr}$ and $\bar{\sigma}_{\theta\theta}$, respectively, in the steady state. Figs. 12 and 13 show the variations of electric and magnetic potential, respectively, in the steady state. From Fig. 11(a) and (b), it is clear that the distribution of the thermal stress $\bar{\sigma}_{rr}$ changes substantially with a change in the parameter R_1 whereas the maximum tensile stress $\bar{\sigma}_{\theta\theta}$ increases with an increase in R_1. It can be seen from Figs. 12 and 13 that the absolute values of electric potential increase and those of magnetic potential decrease with an increase in R_1.

4. Conclusion

In this study, we obtained the exact solution of the transient thermal stress problem of a multilayered magneto-electro-thermoelastic hollow sphere under uniform surface heating as a spherically symmetric state. As an illustration, we carried out numerical calculations for a two-layered hollow sphere composed of piezoelectric and magnetostrictive materials and examined its behavior in the transient state in terms of temperature change, displacement, stress, and electric and magnetic potential distributions. Furthermore, the effects of the stacking sequence and position of the interface were investigated. Though numerical calculation were carried out for a two-layered hollow sphere, numerical calculation for multilayered magneto-electro-thermoelastic hollow sphere with an arbitrary number of layer and arbitrary stacking sequence can be carried out. The present solution can serve as a benchmark to the analysis of magneto-electro-thermoelastic hollow sphere based on various numerical methods.

References

[1] G. Harrshe, J.P. Dougherty, R.E. Newnhan, Theoretical modeling of multilayer magnetoelectric composite, Int. J. Appl. Electromagn. Mater. 4 (1993) 145–159.
[2] C.W. Nan, Magnetoelectric effect in composites of piezoelectric and piezomagnetic phases, Phys. Rev. B50 (1994) 6082–6088.
[3] Y. Benveniste, Magnetoelectric effect in fibrous composites with piezoelecric and piezomagnetic, Phases. Phys. Rev. B 51 (1995) 16424–16427.
[4] C.W. Nan, M.I. Bichurin, S. Dong, D. Viehland, G. Srinivasan, Multiferroic magnetoelectric composites: historical perspective, status, and future directions, J. Appl. Phys. 103 (2008) 031101.
[5] E. Pan, Exact solution for simply supported and multilayered magneto-electro-elastic plates, Trans. ASME J. Appl. Mech. 68 (2001) 608–618.
[6] E. Pan, P.R. Heyliger, Exact solutions for magneto-electro-elastic laminates in cylindrical bending, Int. J. Solids Struct. 40 (2003) 6859–6876.
[7] M.H. Babaei, Z.T. Chen, Exact solutions for radially polarized and magnetized magnetoelectroelastic rotating cylinders, Smart Mater. Struct. 17 (2008) 025035.
[8] J. Ying, H.M. Wang, Magnetoelectroelastic fields in rotating multiferroic composite cylindrical structures, J. Zhejiang Univ. Sci. A 10 (2009) 319–326.
[9] R. Wang, Q. Han, E. Pan, An analytical solution for a multilayered magneto-electro-elastic circular plate under simply supported lateral boundary conditions, Smart Mater. Struct. 19 (2010) 065025.
[10] H.M. Wang, H.J. Ding, Transient responses of a magneto-electro-elastic hollow sphere for fully coupled spherically symmetric problem, Eur. J. Mech. A/Solids 25 (2006) 965–980.
[11] H.M. Wang, H.J. Ding, Radial vibration of piezoelectric/magnetostrictive composite hollow sphere, J. Sound Vib. 307 (2007) 330–348.
[12] R. Anandkumar, R. Annigeri, N. Ganesan, S. Swarnamani, Free vibration behavior of multiphase and layered magneto-electro-elastic beam, J. Sound Vib. 299 (2007) 44–63.
[13] M. Sunar, A.Z. Al-Garni, M.H. Ali, R. Kahraman, Finite element modeling of thermopiezomagnetic smart structures, AIAA J. 40 (2001) 1846–1851.
[14] A. Kumaravel, N. Ganesan, R. Sethurraman, Steady-state analysis of a three-layered electro-magneto-elastic strip in a thermal environment, Smart. Mater. Struct. 16 (2007) 282–295.
[15] P.F. Hou, T. Yi, L. Wang, 2D general solution and fundamental solution for orthotropic electro-magneto-elastic materials, J. Therm. Stresses 31 (2008) 807–822.

[16] P.F. Hou, A.Y. Leung, H.J. Ding, A point heat source on the surface of a semi-infinite transversely isotropic electro-magneto-thermo-elastic material, Int. J. Eng. Sci. 46 (2008) 273–285.
[17] S.M. Xiong, G.Z. Ni, 2D green's functions for semi-infinite transversely isotropic electro-magneto-thermo-elastic composite, J. Magnetism Magn. Mater. 321 (2009) 1867–1874.
[18] C.F. Gao, H. Kessler, H. Balke, Fracture analysis of electromagnetic thermoelastic solids, Eur. J. Mech. A/Solids 22 (2003) 433–442.
[19] B.L. Wang, O.P. Niraula, Transient thermal fracture analysis of transversely isotropic magneto-electro-elastic materials, J. Therm. Stresses 30 (2007) 297–317.
[20] Y. Ootao, Y. Tanigawa, Transient analysis of multilayered magneto-electro-thermoelastic strip due to nonuniform heat supply, Comp. Struct. 68 (2005) 471–480.